A Study on the Effects of Cold Deformation on CMnSi Steel Structures Utilised in the Shipbuilding Industry

Van Nhanh Nguyen (ID) [1]
Duong Nam Nguyen (ID) [2]
Janusz Kozak [3]
Xuan Phuong Nguyen [4]
Dinh Tuyen Nguyen (ID) [4] *

[1] Institute of Engineering, HUTECH University, Ho Chi Minh City, Viet Nam

[2] School of Mechanical Engineering, Vietnam Maritime University, Haiphong, Viet Nam

[3] Gdansk University of Technology, Institute of Naval Architecture, Gdansk, Poland

[4] PATET Research Group, Ho Chi Minh city University of Transport, Ho Chi Minh city, Viet Nam

* Corresponding author: *dinhtuyen.nguyen@ut.edu.vn (D. T. Nguyen)*

ABSTRACT

This article analyses the effects of deformation on the structure of CMnSi steel at various deformation levels. After hot forging, the structure of CMnSi steel comprises coarse-sized alpha and pearlite particles. The average grain size of steel after forging was 100 µm. After hot rolling, the grain size gradually decreases, with the average size of the ferrite and pearlite grains measured as 60 µm. After that, CMnSi steel was subjected to cold deformation at levels of 40%, 60%, and 80%. The grain size of the CMnSi steel sample after 80% cold deformation reached level 7, corresponding to about 25 µm. For a deformation level of 40%, the grain size was level 5, corresponding to 40 µm, while a deformation level of 60% produced a grain size of 35 µm, corresponding to level 6. In addition, scanning electron microscopy showed that after 80% deformation, smaller particles with a size of about 5 µm appear inside the parent particles. Moreover, energy-dispersive X-ray spectroscopy analysis revealed the carbide appearance in the form M23C6, with M being a mixture of Fe and Mn. These carbides have a fine size of about 1–2 µm and contribute to the prevention of particle growth during subsequent heat treatments.

Keywords: CMnSi steel; alpha phase; deformation; carbide; shipbuilding steel

INTRODUCTION

Currently, the world's metallurgical industry is aiming to develop steel that is more durable and flexible, with lower prices and more environmentally friendly technology. Indeed, there are a large number of materials-related technologies that have been studied and developed aiming to enhance efficiency, as well as improve the applicability of these materials to industry [1]–[4]. In the shipbuilding industry, research and production of high-strength steel is required as the application of high-strength steel in shipbuilding could increase the carrying capacity of ships [5], [6]. At the end of the 20th century, the global steel industry experienced many technological revolutions, enhancing the quality of steel. These include the direct reduction of iron ore aiming to produce reduced cast iron products, including sponge iron with low C and P contents, as well as a reduction in S impurities; technology for electric furnace steelmaking and secondary refining to significantly remove impurities; continuous casting technology; and thermomechanical technology aiming to create special structures with enhanced mechanical properties [7], [8]. Among these, advanced high-strength steel (AHSS) is of particular interest, including dual-phase steel (DP), transformation-induced plasticity steel (TRIP), and (TRIP)-aided bainitic ferrite steel (TBF) [9], [10].

AHSS steel belongs to the CMnSi low alloy steel group, with a C content of up to 0.4%, a Mn content ranging from 1% to 2.5%, and a Si content of up to 2.2%. Other elements, such as Cr, Al, Ti, Nb, and V, may also be present. As reported, AHSS has high

cleanliness, in which the required P and S content (P < 0.025%, S < 0.015%) is much lower than HSLA steel [11]. P and S are two elements that are very harmful to steel, causing cracking during mechanical work and reducing the overall mechanical properties. Thus, P and S should be thoroughly removed from the steel [12], [13]. Furthermore, very low amounts of non-metallic impurities and gases (O_2, H_2, N_2) are required to produce AHSS steel with superior properties. Thus, to ensure the mechanical properties and the chemical composition of AHSS steel, it is necessary to use special steelmaking technology [14]–[17]. AHSS steel is strain-hardened by the multiphase structure effect combined with traditional durability principles, such as solid solution durability, dispersed phase secretion, and grain reduction. Thus, by alloying with suitable elements, in combination with impact technology aiming to change the structure and create high-strength solid bainite/martensite phases, the residual austenite is dispersed within a flexible ferrite matrix that has a small grain size (≤ 20 μm) along with isolated phases (i.e., martensite, residual austenite with a grain size ≤ 5 μm). The ferrite phase plays a bonding role, controlling the ductility of steel, while the solid phases act as reinforcing molecules, influencing the durability and ductility of steel.

As a type of AHSS, DP steel has a two-phase structure composed of ferrite and martensite, in which the martensite phase is in the isolated form, accounting for about 10%–40% of the total microstructure and is evenly distributed on the ferrite base. The main alloying elements used in DP steel are C, Mn, Si, and Cr. TRIP steel has a three-phase structure of ferrite, bainite, and residual austenite. Residual austenite, which makes up at least 5% of the total microstructure, is a carbon-rich phase (~1% C) that is evenly distributed in the ferrite/bainite matrix. In addition, there may be a small amount of martensite (≤ 5%), depending on the technological process [18]. The typical structure of TRIP is 50%–60% ferrite, 25%–40% bainite, and about 5%–20% residual austenite. TBF steel has a multiphase structure depending on the heating temperature. If heated above Ms (martensite start) temperature Ms, the obtained TBF is composed of the pro-eutectoid ferrite, bainite-ferrite, and residual austenite phase [19]. If heated below temperature Ms, the obtained TBF is composed of the pro-eutectoid ferrite, bainite-ferrite, residual austenite, and martensite phases. The outstanding mechanical properties of TBF steel are obtained by adjusting the alloying element composition and processing technology. Generally, increasing the C and Mn contents increases the strength of TBF steel but decreases the elongation. Increasing the Si content has the effect of increasing both durability and elongation, along with the durability coefficient. This effect of Si is due to an indirect effect on the structure, mainly making austenite redundant, resulting in increasing durability and plasticity. The effect of Si in TBF steel is completely different from HSLA steel. For HSLA steel, an increased Si content increases steel strength; however, ductility and toughness decrease sharply. In general, C, Mn, and Si not only play critical primary roles but also interact with each other, thus affecting the structure and mechanical properties of TBF steel.

In the literature, there are many studies on TBF steel, primarily utilising C, Mn, and Si. These works mainly focus on studying the cooling deformation process of CMnSi steel and the subsequent effects of these cooling deformation processes on the mechanical properties of CMnSi steel [20], [21]. Some authors have researched the effects of heat treatment conditions on the structure and mechanical properties of CMnSi steel. In addition, they have shown the influence of the final structure (after completing heat treatments) on the mechanical properties of CMnSi steel [22]–[24]. Unfortunately, there are not many studies analysing the effects of varied hot rolling conditions on the structure and mechanical properties of CMnSi steel [25]. However, this hot rolling process is just the preparation stage for the next cold deformation process of CMnSi steel. Some authors have presented research on the effects of some trace elements, including Nb, Cu, and W, on the microstructure and mechanical properties of TBF steel [26]–[28]. These studies have shown the influence of alloying elements on the microstructural formation process and mechanical properties of CMnSi steel. However, there has been no study investigating the effects of cold deformation on the structure of CMnSi steel, even though the cold deformation stage has important consequences regarding the microstructure and properties of steel. Therefore, in this work, we study the influence of the degree of cold deformation on the microstructure of CMnSi steel, with special attention given to the grain size and carbide phases.

MATERIALS AND METHODS

In this work, CMnSi steel with a C concentration in the range of 0.2%–0.24%, Mn in the range of 1.5%–2%, and Si in the range of 1.4%–1.6% was used. The impurity content was very low, in accordance with AHSS steel standards (P ≤ 0.025%, S ≤ 0.015%). Additionally, the gas content was very low (O, H, N). These compositions in CMnSi steel are guaranteed by the refining process. The composition of the CMnSi steel sample is given in Table 1.

Tab. 1. CMnSi steel composition (mass %)

C	Si	S	P	Mn	Ni	Cr	Mo	Cu	W
0.2200	1.6007	0.0089	0.0212	1.3978	0.0456	0.0101	0.0062	0.0399	0.0046

To evaluate the effects of the degree of cold deformation on the microstructure of the CMnSi steel, the sample is prepared as follows:

– After casting, the billet is cut into blocks with a cross-sectional size of 80 * 70 mm and annealed to generate a uniform composition, addressing the segregation that occurred during casting. In this phase, the sample is annealed at 1000 °C for 3 hours.

– After annealing, the steel billet is hot forged with a forging ratio of y = 4 to eliminate casting structures. Steel billets are forged into plates 20 mm thick with a width of 70 mm. The forging starting temperature is about 1200 °C and ends at about 900 °C.

–After forging, the steel billet is hot rolled. The hot rolling mode is designed to ensure that a small, even grain size is obtained, consistent with the equipment's capabilities. Specifically, the total thickness reduction is 50%, producing a billet that is 10 mm thick. The starting temperature for each rolling pass is 920 °C (austenite transformation (Ac_3) + 50 °C), while the temperature of the outside surface of the billet after being

released from the rolling shaft is about 880 °C, as measured by a pyrometer.

– After hot deformation, the steel billet is cold rolled at different degrees of cold deformation, i.e., 40%, 60%, and 80%, ensuring that the sample after deformation has a thickness of 2 mm. Steel samples after cold deformation were analysed using a VHX6800 optical microscope.

RESULTS AND DISCUSSION
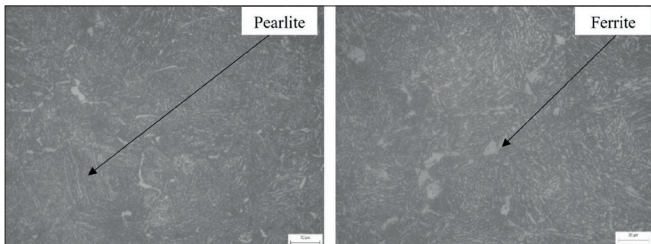
MICROSTRUCTURE OF CMNSI STEEL AFTER HOT ROLLING

Fig. 1. Microstructure of CMnSi steel after forging

Analysis of the microstructure after forging shows that the structure of the CMnSi steel does not have casting defects. After forging, the microstructure of CMnSi steel is stable, facilitating the subsequent deformation process. However, the microstructure consists of coarse light-coloured ferrite particles dispersed within a sheet-like perlite matrix, as shown in Fig. 1. The grain size after forging is quite large, measuring about 80–100 μm. As reported in the literature, the coarse grain size will affect the mechanical properties of the steel, especially durability and ductility. This result is similar to the research of Zhu et al. [23], who reported the formation of ferrite and pearlite phases in the microstructure of CMnSi steel. In their research, they also highlighted the role of these phases in forming the structure following heat treatment of CMnSi steel. Similarly, Kliber et al. [29] and Cooman et al. [30] also showed that the phase structure of CMnSi steel after forging resembles that of the annealed state. However, as key difference lies in the uniformity of phase sizes. After forging, the phases are more uniform in size compared to after annealing. This uniformity in phase size is the most significant distinction between the microstructures resulting from forging and annealing.
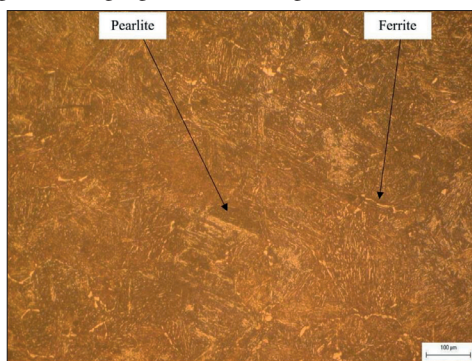

Fig. 2. Microstructure of CMnSi steel after hot rolling

Analysis of the microstructure of CMnSi steel after hot rolling shows that it consists of pearlite particles with a smaller size (~60 μm) compared to the sample after forging. Around the pearlite grain boundary, a dispersed light-coloured alpha structure, which is finer and smaller in size compared to the sample after forging, is observed (Fig. 2). Thus, the hot-rolling process also creates a suitable microstructure for the subsequent cold deformation process. Scanning electron microscopy (SEM) image analysis of CMnSi steel after hot rolling indicates the plate-like pearlite structure, as shown in Fig. 3.
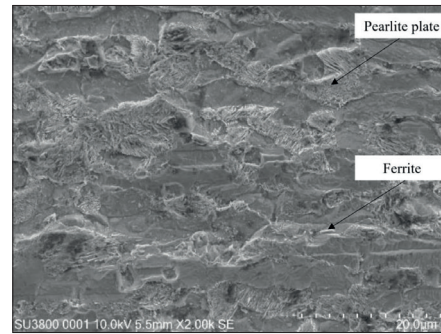

Fig. 3. SEM of CMnSi steel after hot rolling

In the study of Tian et al. [25], the structure of TRIP steel was also shown to have the same composition as the CMnSi steel. They found that the microstructure of TRIP steel includes ferrite phases, residual austenite, and isolated areas of martensite-austenite and bainite. However, they only studied the structure of steel after hot rolling and subsequent heat treatment at 400 °C, without examining the structural development during the hot rolling stage. In contrast, the current work analyses the structure and phase characteristics after hot rolling, a critical step in preparing the structure for subsequent cold deformation. Typically, an uniform dispersion and grain size will determine the size and structure of phases after cold deformation.

MICROSTRUCTURE OF CMNSI STEEL AFTER DEFORMATION

Analysis of the microstructure of the CMnSi steel sample after 40% cold deformation shows that the structure of CMnSi steel consists of α particles (light colour) and pearlite particles (dark colour) that are evenly dispersed, as shown in Fig. 4. These particles are smaller and finer in size compared to those present after hot rolling. The preparation of the CMnSi steel structure with a small grain size is beneficial for subsequent heat treatments. Indeed, the structure after cold deformation has an increased number of grain boundaries, thereby increasing the mechanical properties of the steel.
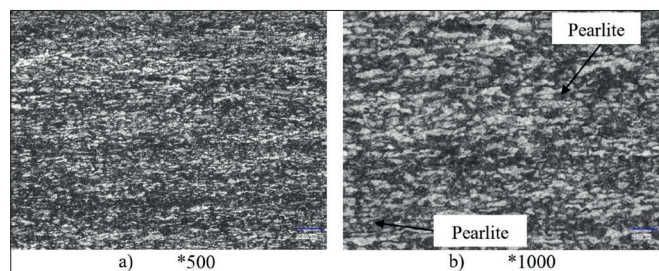

Fig. 4. CMnSi steel sample after 40% deformation

Analysis of the microstructure of the CMnSi steel sample after 60% and 80% deformation shows that the degree of deformation of the sample increases and the grain size of the sample decreases, as illustrated in Fig. 5 and Fig. 6. The cold deformation process also generates more evenly rounded grains compared to the samples after forging and hot rolling. At an 80% deformation level, the grains are fine and evenly distributed, with an average grain size of about 25 µm, compared to 35 µm for samples deformed at 60%. Overall, the high degree of cold deformation results in the appearance of very small, finely sized particles that are evenly dispersed throughout the microstructure.
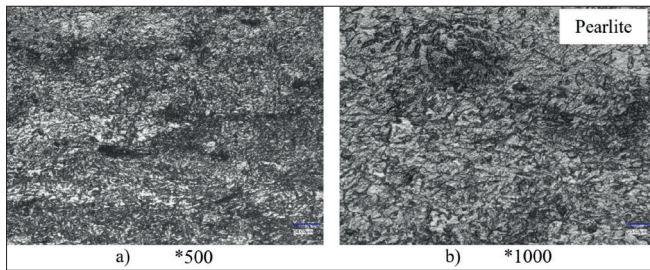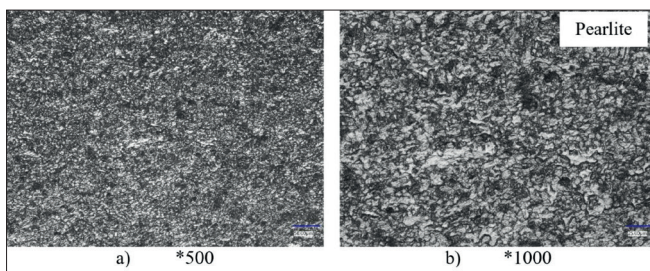

Fig. 5. CMnSi steel sample after 60% deformation

Fig. 6. CMnSi steel sample after 80% deformation

Some existing studies assess how the degree of deformation influences the microstructure of CMnSi steel [25], [31], [32]. These studies generally show that as the degree of cold deformation increases, the grain size after deformation and heat treatment decreases. However, these studies often focus on the final results of various heat treatment modes, without thoroughly investigating the preparation stage (cold deformation stage). Indeed, they do not show how the morphology and phase distribution of the structure change before heat treatment.

Grain size analysis of CMnSi steel at different deformation levels shows that after 40% deformation, the CMnSi steel sample has an average grain size of level 5, corresponding to about 40 µm (Fig. 7). At a deformation level of 60%, the average grain size is level 6, corresponding to a grain size of about 35 µm, as depicted in Fig. 8. When the deformation level is increased to 80%, the average grain size is level 7, corresponding to about 25 µm, as shown in Fig. 9. Additionally, the microstructure of the sample after extensive deformation features fine, small-sized particles that are evenly dispersed within the CMnSi steel matrix.
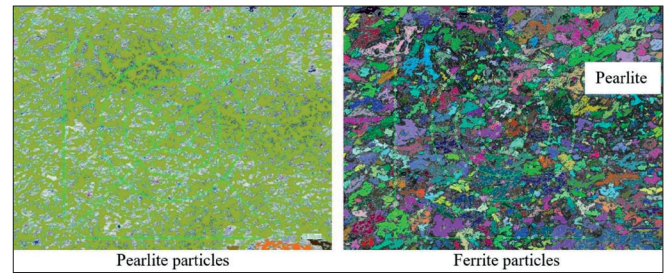

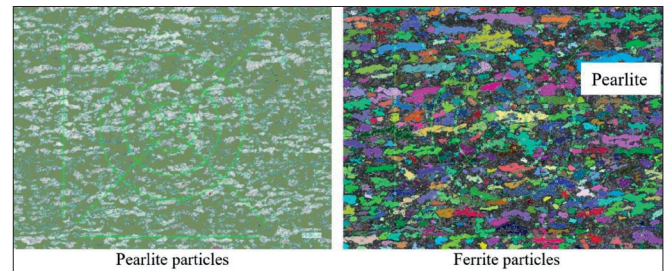Fig. 7. Average grain size of CMnSi steel sample after 40% deformation

Fig. 8. Average grain size of CMnSi steel sample after 60% deformation
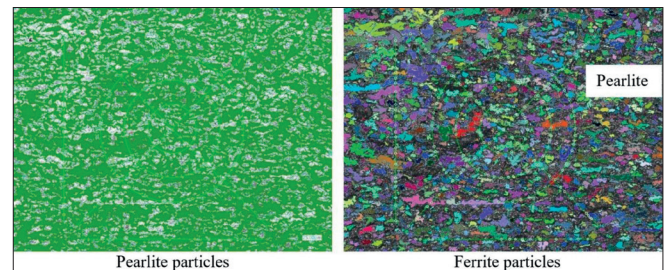

Fig. 9. Average grain size of CMnSi steel sample after 80% deformation

As shown in Fig. 10, increasing the degree of cold deformation creates fine and small-sized particles. These particles are evenly dispersed in the matrix, consequently enhancing the mechanical properties after heat treatment. This phenomenon can be attributed to the significant energy accumulation during extensive deformation, facilitating subsequent heat treatment processes. Indeed, small-sized particles increase the number of accumulated boundaries and the number of nucleation centres for subsequent heat treatments. A high degree of deformation will increase the accumulation of dislocations at grain boundaries, contributing to the stabilization process of steel.
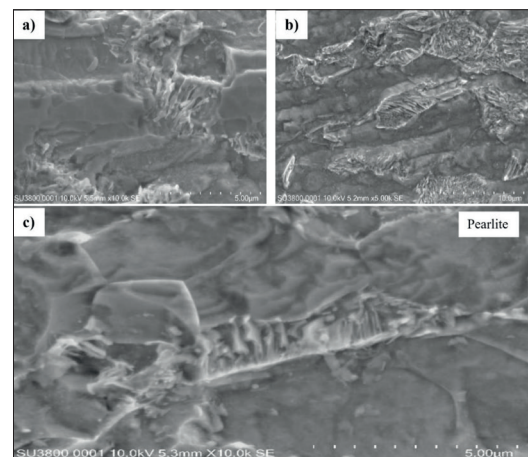

Fig. 10. SEM analysis of CMnSi steel sample after deformation; a) 40% deformation, b) 60% deformation, and c) 80% deformation

Analysis of the microstructure after deformation to varying degrees shows that increasing deformation levels gradually reduce the grain size, corroborating findings from optical microscopy analysis. However, SEM image analysis shows that increasing the deformation level to 80% creates fine particles with a size of less than 5 µm. Furthermore, within the microstructure, the presence of carbide-like particles comprising Mn, Si, and Fe along with C is discernible, a conclusion supported by energy-dispersive X-ray spectroscopy (EDS) analyses, as depicted in Fig. 11 and detailed in Table 2.
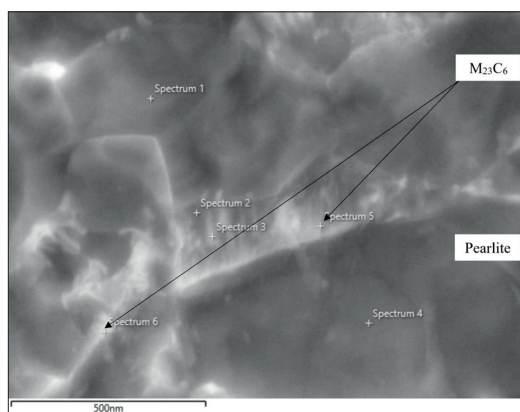

Fig. 11. EDS analysis of CMnSi steel sample after 80% deformation

Upon examining Spectra 5 and 6, it becomes evident that carbides consisting of Mn, Si, Fe, and C are present. From the analysis in Table 2, it shows that these carbides are located mainly in the grain boundary regions. Notably, these carbide grains serve a pivotal role in impeding grain development during heat treatments, as illustrated in Fig. 12.
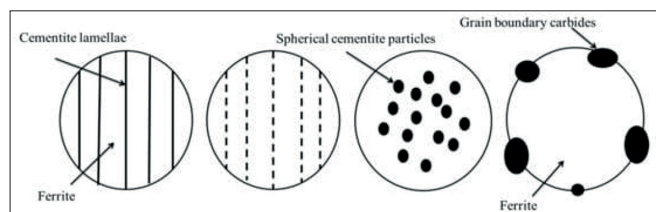

Fig. 12. Strengthening mechanism of CMnSi steel through grain boundary [33]

The findings of this study align closely with previous research investigating the impact and significance of carbides on grain development during subsequent heat treatments [18],[20],[21] [22],[23]. The study by Hojo et al. [34] showed the influence of NbC carbides on the microstructural formation of steel after heat treatment. The investigations by Kowalski et al. [35], [36] highlighted the substantial influence of material thickness on mechanical properties, particularly in terms of brittle fracture mechanisms. Wang et al. [33] underscored the contribution of certain carbides to the steel hardening process.

In the structural evolution of steel after forging, hot rolling, and cold deformation, the presence of carbides at grain boundaries is notable. These carbides serve as catalysts for the steel's hardening process during heat treatments. The carbides are dispersed both at the grain boundaries and in the steel matrix, with an average size of 1–2 µm. They are believed to act as nucleation sites, facilitating

Tab. 2. Composition of elements in CMnSi steel at various points in the microstructure after 80% deformation

Element	Line Type	Weight %	Weight % sigma	Atomic %
Spectrum 1				
C	K series	2.92	0.36	11.98
Si	K series	2.60	0.08	4.56
Mn	K series	1.52	0.14	1.36
Fe	K series	92.96	0.38	82.10
Spectrum 2				
C	K series	3.81	0.36	15.31
Si	K series	1.84	0.07	3.17
Mn	K series	2.46	0.16	2.16
Fe	K series	91.88	0.38	79.36
Spectrum 3				
C	K series	5.24	0.37	20.16
Si	K series	1.68	0.07	2.77
Mn	K series	2.57	0.16	2.17
Fe	K series	90.51	0.39	74.91
Spectrum 4				
C	K series	3.27	0.38	13.26
Si	K series	2.84	0.09	4.91
Mn	K series	1.51	0.14	1.34
Fe	K series	92.38	0.39	80.49
Spectrum 5				
C	K series	7.60	0.39	27.30
Si	K series	1.71	0.07	2.63
Mn	K series	2.50	0.15	1.96
Fe	K series	88.19	0.41	68.11
Spectrum 6				
C	K series	9.23	0.42	31.69
Si	K series	1.75	0.07	2.57
Mn	K series	2.75	0.16	2.06
Fe	K series	86.26	0.43	63.68

the recrystallization process to strengthen the steel during heat treatments. In addition, carbides at the grain boundaries will prevent grains from growing during the heat treatment stage. These carbide particles have a similar structure to M23C6, in which M is a mixture of Fe and Mn metals.

CONCLUSION

This work shows the structural changes of CMnSi steel exposed to a variety of deformation modes. Following forging, the CMnSi steel sample exhibits light-coloured alpha particles and coarse pearlite, with sizes reaching about 100 µm. After hot rolling, the microstructure consists of pearlite plates with a grain size of about 60 µm. Additionally, the alpha particles are more evenly dispersed in the matrix. After cold deformation, the grain size becomes smaller. Furthermore, with increasing deformation, it is found that the grain size gradually decreases, while fine and small-sized particles

are dispersed throughout the CMnSi steel matrix. With a cold deformation level of 40%, the granularity is level 5, corresponding to a grain size of 40 μm. When the cold deformation level is 60%, the granularity is level 6, corresponding to a grain size of 35 μm. For a cold deformation level of 80%, the granularity is level 7, corresponding to a grain size of about 25 μm. In addition, particles with a size smaller than about 5 μm were observed inside the parent particles at a deformation level of 80%. SEM and EDS revealed the presence of carbide particles dispersed in the matrix, while some complex M23C6 carbide particles are formed at grain boundaries. These carbide particles, typically measuring about 1–2 μm, serve to strengthen the grain boundary and act as nucleation sites for the recrystallization process.

ACKNOWLEDGEMENT:

REFERENCES

1. Abid M, Kchaou M, Hoang AT, Haboussi M. Wear Mechanisms Analysis and Friction Behavior of Anodic Aluminum Oxide Film 5083 under Cyclic Loading. J Mater Eng Perform 2024;33:1527–1537. https://doi.org/10.1007/s11665-023-08616-8.

2. George JS, Vijayan P P, Hoang AT, Kalarikkal N, Nguyen-Tri P, Thomas S. Recent advances in bio-inspired multifunctional coatings for corrosion protection. Prog Org Coatings 2022;168:106858. https://doi.org/10.1016/j.porgcoat.2022.106858.

3. Hoang AT, Tran TT Van, Nguyen VB, Nguyen DN. Effect of Heat Treatment Process on The Microstructure and Mechanical Properties of The Spray Coating Ni-Cr on CT38 Steel. Int J Adv Sci Eng Inf Technol 2019;9:560–568. https://doi.org/10.18517/ijaseit.9.2.7891.

4. Thi H, Quyen N, Tuan VA, Dong TP, Quyen VV, Nam ND. Effect of Rare Earth on M7C3 Eutectic Carbide in 13 % Chromium Alloy Cast Iron. Int J Adv Sci Eng Inf Technol 2019;9:724–728.

5. Liu D, Li Q, Emi T. Microstructure and mechanical properties in hot-rolled extra high-yield-strength steel plates for offshore structure and shipbuilding. Metall Mater Trans A 2011;42:1349–1361.

6. Wang S, Dai J, Wang J, Li R, Wang J, Xu Z. Numerical calculation of high-strength-steel saddle plate forming suitable for lightweight construction of ships. Materials (Basel) 2023;16:3848.

7. Backman J, Kyllönen V, Helaakoski H. Methods and tools of improving steel manufacturing processes: Current state and future methods. IFAC-PapersOnLine 2019;52:1174–9.

8. Geng X, Wang F, Wu H, Wang S, Wu G, Gao J, et al. Data-driven and artificial intelligence accelerated steel material research and intelligent manufacturing technology. Mater Genome Eng Adv 2023;1:e10.

9. Kučerová L, Jirková H, Mašek B. Continuous Cooling of CMnSi TRIP Steel. Mater Today Proc 2015;2:S677–680. https://doi.org/10.1016/j.matpr.2015.07.374.

10. Feng X, Liu X, Bai S, Tang Y, Ye Y. Investigation of dynamic tensile mechanical responses and deformation mechanism at high strain rates in a TWIP steel. J Mater Res Technol 2023;26:639–653. https://doi.org/10.1016/j.jmrt.2023.07.241.

11. Mintz B, Qaban A, Kang SE. The Influence of Small Additions of Alloying Elements on the Hot Ductility of AHSS Steels: A Critical Review Part 2. Metals (Basel) 2023;13:406.

12. Chen Z, Gu J, Han L. Bainite Transformation Characteristics of High-Si Hypereutectoid Bearing Steel. Metallogr Microstruct Anal 2018;7. https://doi.org/10.1007/s13632-017-0410-5.

13. Hasan SM, Kumar S, Chakrabarti D, Singh SB. Effect of prior austenite grain size on the formation of carbide-free bainite in low-alloy steel. Philos Mag 2020;100. https://doi.org/10.1080/14786435.2020.1764653.

14. Leach L. Modeling Bainite Formation in Steels. KTH Royal Institute of Technology; 2018.

15. Morawiec M, Ruiz-Jimenez V, Garcia-Mateo C, Grajcar A. Thermodynamic analysis and isothermal bainitic transformation kinetics in lean medium-Mn steels. J Therm Anal Calorim 2020;142:1709–1719. https://doi.org/10.1007/s10973-020-10259-z.

16. Rodrigues KF, Mourão GMM, Faria GL. Kinetics of Isothermal Phase Transformations in Premium and Standard Rail Steels. Steel Res Int 2021;92. https://doi.org/10.1002/srin.202000306.

17. Hendi SH, Panahiyan S, Panah BE, Jamil M. Alternative approach to thermodynamic phase transitions. Chinese Phys C 2019;43. https://doi.org/10.1088/1674-1137/43/11/113106.

18. Park J, Min KM, Kim H, Hong S, Lee M. Integrated Computational Materials Engineering for Advanced Automotive Technology: With Focus on Life Cycle of Automotive Body Structure. Adv Mater Technol 2023;8. https://doi.org/10.1002/admt.202201057.

19. Nguyen VN, Nguyen AX, Nguyen DT, Le HC, Nguyen VP. A Comprehensive Understanding of Bainite Phase Transformation Mechanism in TRIP Bainitic-supported Ferrite Steel. Int J Adv Sci Eng Inf Technol 2024;14:309–325. https://doi.org/10.18517/ijaseit.14.1.19706.

20. Van HD, Van CN, Ngoc TT, Manh TS. Influence of heat treatment on microstructure and mechanical properties of a CMnSi TRIP steel using design of experiment. Mater Today Proc 2018;5:24664–24674. https://doi.org/10.1016/j.matpr.2018.10.264.

21. Fu YT, Liu J, Shi J, Cao WQ, Dong H. Effects of Cold Rolling Reduction on Retained Austenite Fraction and Mechanical Properties of High-Si TRIP Steel. J Iron Steel Res Int 2013;20:50–56. https://doi.org/10.1016/S1006-706X(13)60097-7.

22. Srivastava AK, Jha G, Gope N, Singh SB. Effect of heat treatment on microstructure and mechanical properties of cold rolled C-Mn-Si TRIP-aided steel. Mater Charact 2006;57:127–135. https://doi.org/10.1016/j.matchar.2006.01.010.

23. Zhu R, Li S, Karaman I, Arroyave R, Niendorf T, Maier HJ. Multi-phase microstructure design of a low-alloy TRIP-assisted steel through a combined computational and experimental methodology. Acta Mater 2012;60:3022–3033. https://doi.org/10.1016/j.actamat.2012.02.007.

24. Sierra R, Nemes JA. Investigation of the mechanical behaviour of multi-phase TRIP steels using finite element methods. Int J Mech Sci 2008;50:649–665. https://doi.org/10.1016/j.ijmecsci.2008.01.005.

25. Tian Y, Li Z. Effects of Warm Deformation on Mechanical Properties of TRIP Aided Fe-C-Mn-Si Multiphase Steel. J Iron Steel Res Int 2012;19:47–52. https://doi.org/10.1016/S1006-706X(12)60126-5.

26. Park HS, Han JC, Lim NS, Park CG. Nano-scale observation on the transformation behavior and mechanical stability of individual retained austenite in CMnSiAl TRIP steels. Mater Sci Eng A 2015;627:262–269. https://doi.org/10.1016/j.msea.2015.01.005.

27. Wang ZC, Kim SJ, Lee CG, Lee TH. Bake-hardening behavior of cold-rolled CMnSi and CMnSiCu TRIP-aided steel sheets. J Mater Process Technol 2004;151:141–145. https://doi.org/10.1016/j.jmatprotec.2004.04.029.

28. Chen XX, Shen J, Kecskes LJ, Wei Q. Tungsten-based heterogeneous multilayer structures via diffusion bonding. Int J Refract Met Hard Mater 2020;92:105308. https://doi.org/10.1016/j.ijrmhm.2020.105308.

29. Kliber J, Mašek B, Zacek O, Staňková H. Transformation Induced Plasticity (TRIP) Effect Used in Forming of Carbon CMnSi Steel. Mater Sci Forum 2005;500–501:461–470. https://doi.org/10.4028/www.scientific.net/msf.500-501.461.

30. De Cooman BC. Structure–properties relationship in TRIP steels containing carbide-free bainite. Curr Opin Solid State Mater Sci 2004;8:285–303.

31. Fu B, Yang W, Li L, Sun Z. Effect of carbon content on microstructure and mechanical properties of cold-rolled C-Mn-Al-Si trip steel. Jinshu Xuebao/Acta Metall Sin 2013;49. https://doi.org/10.3724/SP.J.1037.2012.00656.

32. Hien D Van. Influence of thermal-mechanical on microstructure and mechanical of TRIP CMnSi steel from foam-iron. Institute of Military Science and Technology, 2018.

33. Wang S, Cao L, Zhang Z. Influence of Carbide Morphology on the Deformation and Fracture Mechanisms of Spheroidized 2019:1–11.

34. Hojo T, Kobayashi J, Kajiyama T, Sugimoto K. Effects of Alloying Elements on Impact Properties of Ultra High-Strength TRIP-Aided Bainitic Ferrite Steels n.d.:9–16.

35. Kowalski J, Kozak J. Numerical model of plastic destruction of thick steel structural elements. Polish Marit Res 2018; 25:78–84.

36. Gu J, Fernandes AC, Chai W, Bu SX, Han X. Analytical and Experimental Investigation of Asymmetric Floating Phenomena of Uniform Bodies. Polish Marit Res 2024; 31:16–23. https://doi.org/doi:10.2478/pomr-2024-0002.